Quasi-static and dynamic characterization of ultrafine-grained 2017A-T4 aluminium alloy processed by accumulative roll bonding

A. HALIMI[1)], A. BOUDIAF[1)], L. HEMMOUCHE[1)], A. MEDJAHED[1)],
D. E. TRIA[2)], A. HENNICHE[1], M. E. A. DJEGHLAL[3)], T. BAUDIN[4)]

[1)] *Laboratoire Génie des Matériaux, École Militaire Polytechnique,*
BP17 Bordj El-Bahri, 16046 Algiers, Algeria, e-mail: halimi.amel.18@gmail.com
(corresponding author), ORCID: 0000-0001-7439-9032

[2)] *Laboratoire Dynamique des Systèmes Mécaniques, École Militaire Polytechnique,*
BP17 Bordj El-Bahri, 16046 Algiers, Algeria

[3)] *LSGM Département de Métallurgie, Ecole Nationale Polytechnique,*
10 Avenue Hassen Badi, BP 182 El Harrach 16200, Alger, Algérie

[4)] *Université Paris-Saclay, CNRS, Institut de Chimie Moléculaire et des Matériaux*
d'Orsay, 91405 Orsay, France

IN THIS STUDY, NOVEL COMPOSITE STRIPS BASED ON 2017A-T4 aluminium alloy (Al-Cu-Mg) produced by accumulative roll bonding (ARB) were developed. The microstructure and mechanical properties of the ultrafine-grained sheets under quasi-static and dynamic loadings were investigated. The initial microstructure characterization with an Optical Microscope and a Scanning Electron Microscope indicated that the ARBed sheets formed a compact material with the homogeneous and identical thickness for the individual bonded layers. Besides, the presence of precipitates was identified in all the processed strips with diverse sizes, quantities and distribution. Moreover, from Electron Back Scatter Diffraction, the microstructure was noticeably refined with increasing the ARB cycles to reach 1.7 µm of the grain size at the fifth cycle. The microhardness measurement and the tensile test were carried out for both natural ageing and ARBed specimens. Accordingly, the tensile stress acts on the individual layers rather than the entire sample that conduct to a reduction in the overall properties for the ARBed strips. Furthermore, a stabilization in the mechanical properties for the three first ARB cycles was noted, whereas, the domination of the dynamic recrystallization was responsible for a significant drop after the fourth cycle which is considered as the transition state. The characteristics of the compression deformation were examined under dynamic and quasi-static loadings conditions by using the Split–Hopkinson Pressure Bar system and the universal testing machine, respectively. The strain hardening behaviour was investigated using the Hollomon analysis. It was found that the thermal softening played a crucial role when compared to the strain hardening for all the studied strips. Moreover, the strain rate under the dynamic loading has a minor effect on the stress flow of the ARBed sheets compared to the as-received material.

Key words: accumulative roll bonding (ARB), 2017A-T4 aluminium alloy, quasi-static loading, dynamic loading, grain refinement.

1. Introduction

THE SEVERE PLASTIC DEFORMATION PROCESS (SPD) consists of applying a large plastic deformation to material through a top-down approach to produce ultrafine-grained structures (UFGs) from the initial coarse-grained material [1–3]. That allows the obtaining of outstanding overall properties according to the Hall–Petch relation [4, 5, 6], which relates to the hardening by refining the grain size.

There are many techniques of SPD [7–10], most of them have come from the adaptation of an existing industrial process such as Accumulative Roll Bonding (ARB) inspired from the rolling process [11, 12], Equal-Channel Angular Pressing (ECAP) derivated from the extrusion technique [13–15], High-Pressure Torsion (HPT) from deformation by torsion and Constrained Groove Pressing (CGP) issue from the forging process [16–18].

The ARB process is an effective way of producing ultrafine-grained (UFG) materials [19–23]. This process has been invented by SAITO *et al.* [24, 20] by adopting a repeated procedure of cutting, stacking and roll-bonding of plates for a desired number of cycles. Besides forming an ultrafine-grained microstructure from alloys and pure metals, this process can be adapted industrially for continuous production of substantial quantities of material contrary to the other SPD techniques [25, 26].

LEE *et al.* [27] demonstrated that shear strain greatly affects the grain refinement by ARB. In their study, they founded a good correspondence between grain size and shear strain. Also, an increase of shear strain redundant with the number of ARB cycles was proved. However, the distribution of shear strain through the thickness became complicated by the number of cycles and location in thickness.

The microstructure of the ARB processed material has a lamellar/pancake structure. This microstructure is due to the redundant shear strain during the ARB process by grain deformation, not by grain subdivision as in the other SPD techniques [28, 29].

The elongated grains formed at large strains are surrounded by high angle grain boundaries (HAGB) and subdivided by low angle grain boundaries (LAGB). The spacing of lamellar boundaries decreased, and the misorientation angle across boundaries increased with increasing the number of ARB cycles. The microstructure of the ARB processed material, especially the lamellar structure, affects the material plastic anisotropy. This microstructure influence was demonstrated by measuring the Lankford parameter, which increased with increasing the number of ARB cycles [30].

Moreover, the UFG microstructure had an impact on the mechanical properties of the ARB processed material [31, 32]. Hardness, yield stress and tensile strength significantly increased proportionately to the number of ARB cycles, unlike the ductility which decreased from the first cycle. LEE [33] and GASHTI [34] found that the rising of hardness had an inhomogeneous distribution through

the thickness. This distribution exhibits a maximum value near the layers' surface due to the shear strain redundant produced from the friction between the rolls and strip surfaces under non-lubricated conditions and the wire brushing before rolling [28]. Besides, the strain hardening of the ARB processed alloy was related to the grain size and dislocation density, where the strain hardening rate increased by the number of ARB cycles [34].

Several studies in the UFG material were focused on mechanical properties enhancement in the quasi-static strain rate domain. However, various applications were related to dynamic loading conditions such as automobile and aeronautic industry. Therefore, the quasi-static mechanical characterization and dynamic properties of UFG materials must be considered and examined in more depth.

There are few studies that explored the dynamic behaviour of UFG aluminium alloys as AA7075 aluminium alloy produced by Expansion Equal Channel Angular Extrusion (Exp-ECAE) [35], Al-26wt.%Si and Al-Zn-Mg alloy produced by Equal Channel Angular Extrusion (ECAP) [36-38], Al-Mg-Mn alloy produced by High-Pressure Torsion (HPT) [39], AA2219 aluminium alloy produced by Multiaxial Forging at Cryogenic Temperature (MFCT) [40] and AA1075 aluminium alloy produced by Accumulative Roll Bonding (ARB) [41]. In these works, the dynamic investigations were performed using the Split Hopkinson Pressure Bar (SHPB) and the shock wave loading technique at the different strain rate varied between 500 and 10^5 s^{-1}. It was reported that the results of dynamic tests for UFG aluminium alloy proceeding by SPD reveal an increase of the dynamic yield stress and the flow stress with increasing the strain rate. Besides, the grain refinement improved the strain rate sensitivity of the alloy. The dynamic proprieties have not been fully explored yet for the ARB processed aluminium–copper based alloys [31, 40].

In the present work, the microstructure evolution and its effects on both quasi-static and dynamic mechanical properties of the ARB processed 2017A-T4 aluminium alloy at various numbers of cycles were studied. The mechanical properties of the as-received material in the natural ageing state are governed by the precipitates strengthening phenomenon. So, from this metallurgical state and proceeding by the ARB technic, the resulting UFG structure's influence and the proceeding conditions on the precipitates evolution so then on the mechanical behaviour were investigated.

2. Results and discussions

2.1. The microstructural characterisation

The number of the individual layers (n_c) after N cycles can be calculated as follows:

$$(2.1) \qquad n_c = 2^N.$$

Figure 1 shows the optical micrographs of the processed specimens from the 1st to the 5th cycles. At each cycle, good bonding with no delamination between strips was under the present ARB conditions. In particular, for the fifth cycle (Fig. 1e), 31 interfaces should be observed $(n_c - 1)$. However, only the last interface and some parts of unbonded interfaces are seen in the full thickness of the specimen.
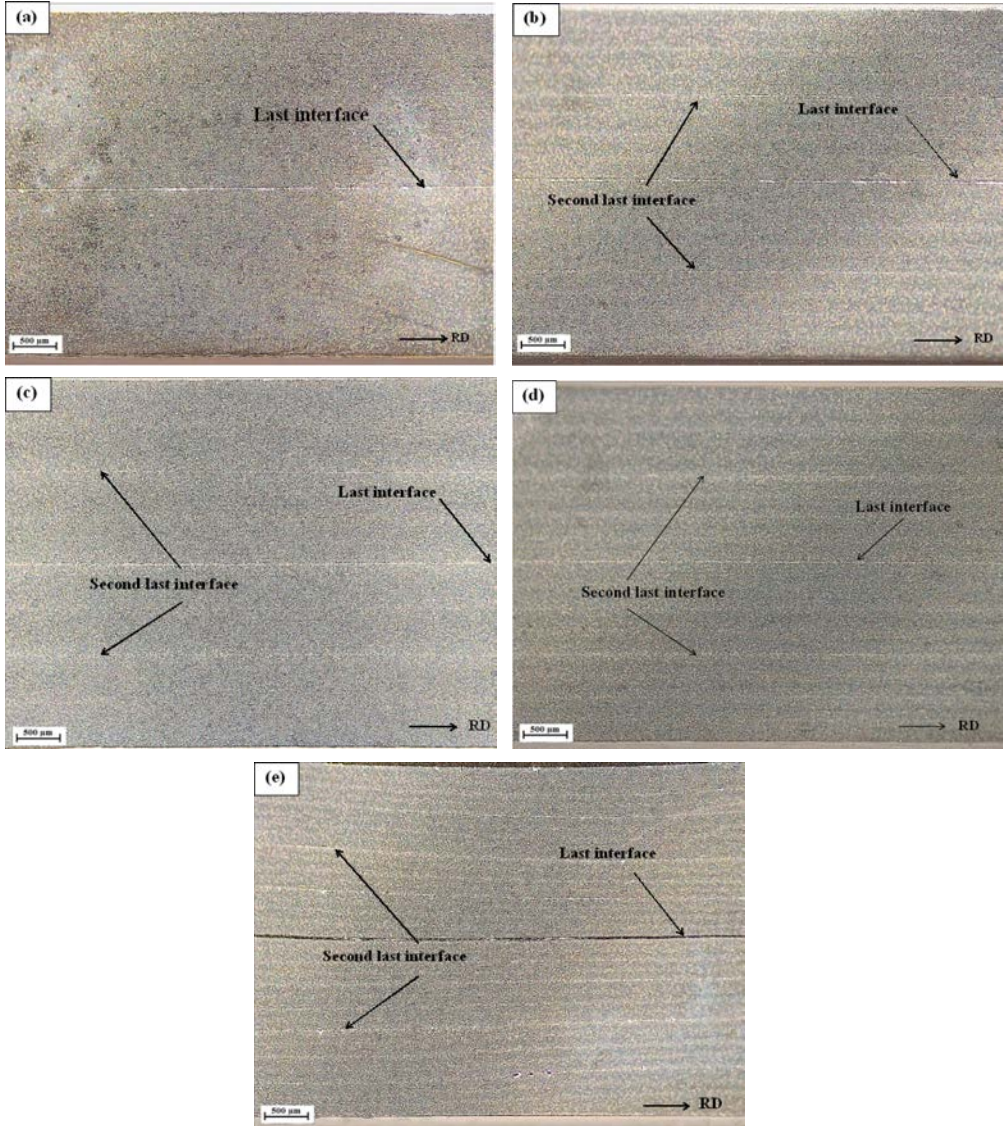

FIG. 1. Optical micrographs of ARBed 2017A aluminium alloy at different number of cycles: a) 1 cycle, b) 2 cycles, c) 3 cycles, d) 4 cycles, and e) 5 cycles (RD = Rolling Direction).
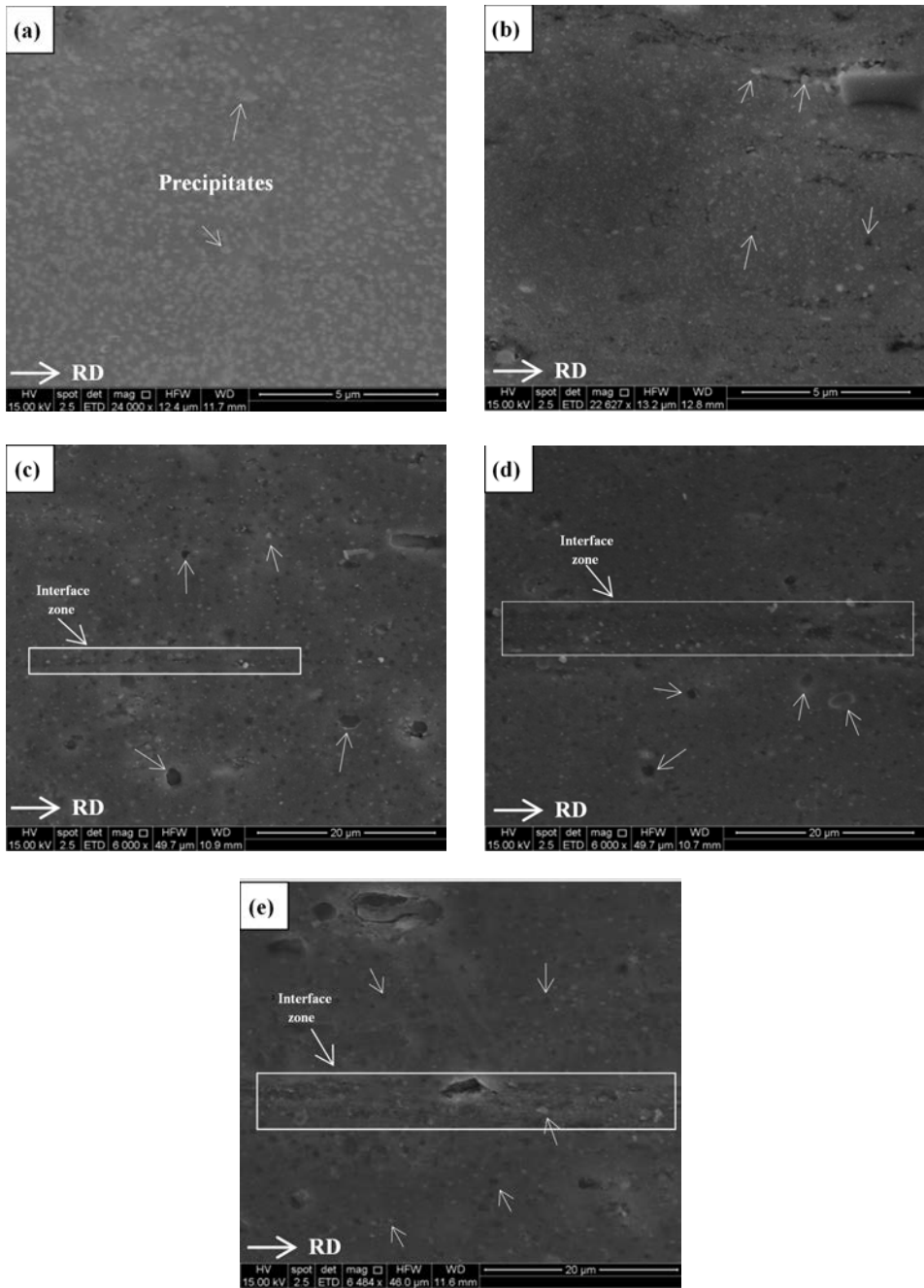
FIG. 2. SEM micrographics of natural ageing and ARBed 2017A aluminium alloy at different number of cycles: a) 1 cycle, b) 2 cycles, c) 3 cycles, d) 4 cycles, and e) 5 cycles (RD = Rolling Direction).

It can be noticed that the individual layers were homogeneous, parallel and having an identical thickness (t). This thickness can be evaluated from

$$(2.2) \qquad\qquad\qquad t = \frac{t_0}{2^N}.$$

Moreover, the interfacial bonding is visible in the samples' centre for each cycle, thus presenting poor bonding and the weakest link in the processed strips due to the application of a single plastic deformation. However, the other interfaces from the previous cycles are difficult to detect or almost indistinguishable when the discontinuities between the sheets were reduced. This results from the important accumulated plastic deformation with increasing the number of cycles. Herein, it can be concluded that the degree of the interfacial bonding quality has been improved to reach metallurgical adhesion between the processed interfaces [20, 33].

Figure 2 illustrates SEM micrographs of a typical cross-section of the ARBed specimens at different cycles. The presence of second-phase particles can be observed in all ARBed sample microstructure, with dissimilarity in size, density, and dispersion. Two types of precipitate: Al_2Cu, Al_2CuMg were identified by EDS analyses (Fig. 3); they are naturally present in the as-received 2017A aluminium alloy in the T4 state [42, 43, 48], and the formation of this kind of precipitates is responsible for the strengthening properties known as the precipitation hardening phenomenon [48]. Furthermore, this precipitate agglomeration zone was located in the last interface, particularly at the three last cycles (Fig. 2c, d, e).
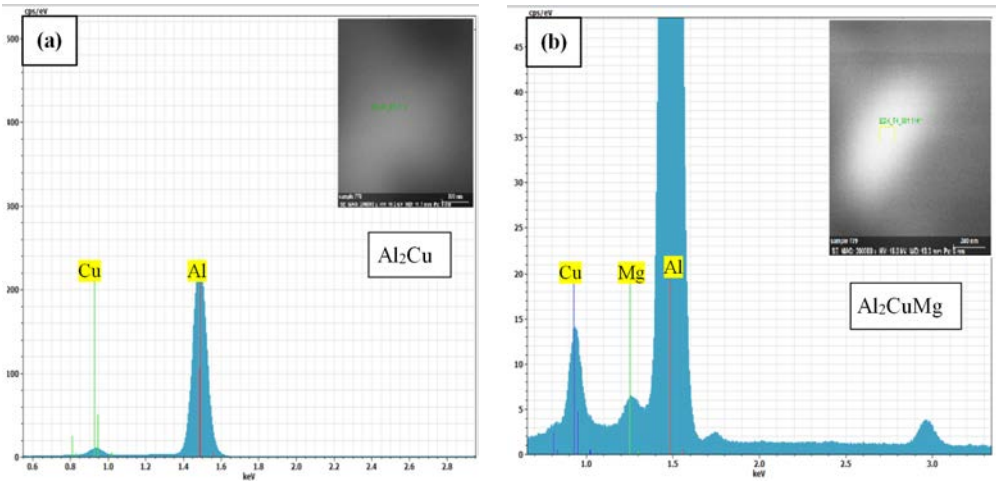

FIG. 3. EDS spectrum of precipitates.

It is clearly observed that with increasing the number of ARB cycles these precipitates become finer, more distant and distributed inhomogeneously in the matrix. This can be explained by the introduction of a fragmentation mechanism during the deformation process, a dissolution phenomenon caused by heat
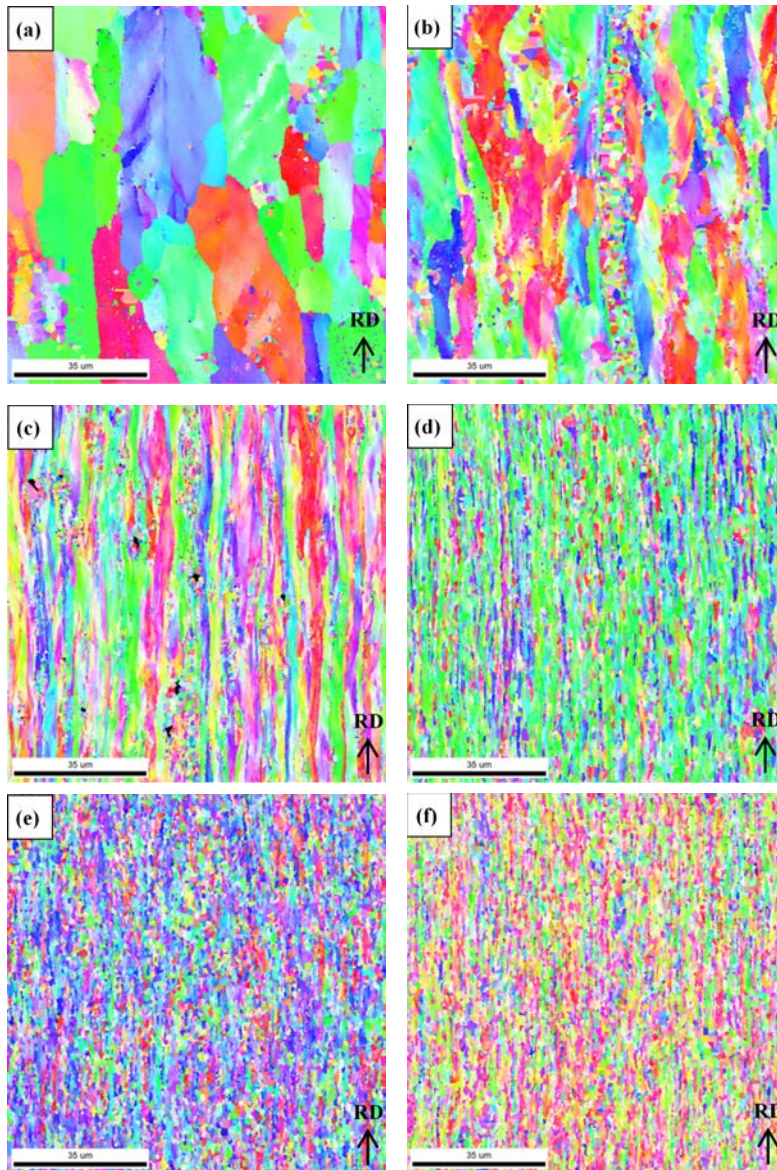

FIG. 4. TD-IPF maps of natural ageing and ARBed 2017A aluminium alloy at different number of cycles: a) natural ageing, b) 1 cycle, c) 2 cycles, d) 3 cycles, e) 4 cycles, and f) 5 cycles.

treatment before rolling, in addition to the converting of the severe plastic deformation energy to thermal energy which leads to the formation of a state close to a solid solution or loss of coherency precipitates – matrix, and finally a continuous deformation process simultaneously with the matrix [45]. Thus, the evolution of precipitates in aluminium alloy 2017A-T4 processed by ARB and the grain refinement mechanism are attributed to the combination of plastic deformation and thermal energy which controlled the motion of dislocations in the function of barriers (grain boundaries and precipitates).

Figure 4 shows the microstructural evolution of the processed specimens obtained from the EBSD analyses. It is clear that there is a grain refinement of ARBed material compared to the natural ageing (Fig. 4a). The plastic deformation is not yet homogeneous in the first ARB cycle, leading to the non-uniform grain size distribution, as illustrated in Fig. 4b [31, 34]. After that, the ultrafine-grained structure becomes more clear (Fig. 4d, e, f) with equiaxed grains, particularly in the interface due to redundant shear strain and the agglomeration of precipitates (Figs. 4b and 7c) [33], and elongated grains in the rolling direction (RD) were formed in most areas of deformed samples and developed a lamellar microstructure. Also, the grain size (Table 1) and the lamellar boundaries spacing decrease with increasing the number of ARB cycles [29].

Table 1. **Grain size measurements of studied strips.**

Specimen	Grain size [μm]
Natural ageing	16.8 ± 1.9
1 cycle	10.8 ± 0.8
2 cycles	7.6 ± 0.4
3 cycles	2.0 ± 0.3
4 cycles	1.7 ± 0.2
5 cycles	1.8 ± 0.2

2.2. Mechanical characterisation

2.2.1. Microhardness measurements. Figure 5 presents the microhardness variations of the as-received alloy and the processed samples at different ARB cycles. The microhardness of the naturally aged alloy reached about 145 Hv. This high microhardness is attributed to the precipitates strengthening phenomena [42–44, 48]. After the first cycle, a remarkable decrease of around 42% was detected compared to the as-received sheets. Although the grain refinement was achieved, as reported in Fig. 4, the processed strips still not hardened as in previous articles [18, 31, 39, 41], this decrease can be assigned to the reduction of size, quantity and distribution of the precipitates caused by plastic deformation and thermal energy during the ARB process (Fig. 2) [45], which reduce the ob-
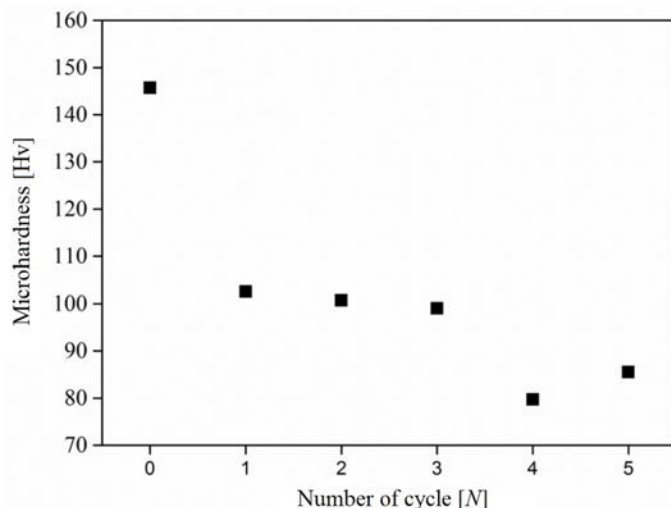
FIG. 5. Evolution of Vickers microhardness of natural ageing ($N = 0$) and ARBed 2017A aluminium alloy at different number of cycles.

stacles against the movement of dislocations. Furthermore, during the first three ARB cycles, the microhardness values revealed practical stability attributed to the saturation in dislocation density caused by the high strain conditions. This hardening behaviour was previously reported in UFG materials manufactured by SPD [31, 46]. Besides, a slight drop in the microhardness was observed after the third cycle. This phenomenon is ascribed to the dynamic recrystallisation mechanism at high strain conditions, leading to reduced grain size and annihilation of dislocations [31]. There is a competition between two main phenomena that control the hardening of ARBed sheets: the dislocation annihilation and dynamic recrystallisation mechanism associated with precipitates behaviour reported above.

2.2.2. Tensile test. The representative engineering stress-strain curves of the studied samples and the corresponding tensile data are presented in Fig. 6 and summarised in Table 2, respectively. The Ultimate Tensile Strength (UTS) decreased from about 458 MPa for the naturally aged sample to reach about 370 MPa after the first cycle, which corresponds to a reduction of around 23%. In contrast, a slight increase in Yield Stress (YS) of around 6% was reported. Further, the processed samples exhibit a decrease in the YS and UTS values from the first cycle gradually to attain a significant drop (51% and 48%, respectively) after the fourth cycle. Besides, a slight increase in strength after five cycles was noticed.
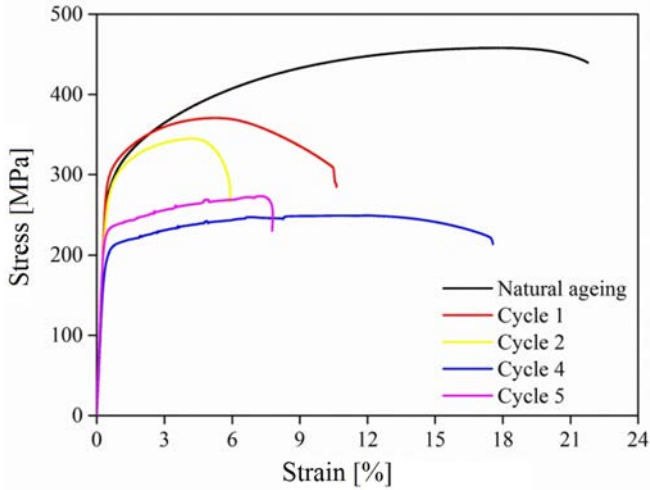
FIG. 6. Tensile engineering stress-strain curves of natural ageing and ARBed 2017A aluminium alloy at different number of cycles.

Table 2. Tensile properties data of studied samples.

Specimen	YS [MPa]	UTS [MPa]	TE [%]
Natural ageing	282 ± 7.4	458 ± 12.3	20 ± 1.3
1 cycle	301 ± 8.1	370 ± 11.4	09 ± 1.0
2 cycles	277 ± 7.2	345 ± 10.9	05 ± 0.9
4 cycles	199 ± 6.5	249 ± 9.6	16 ± 1.1
5 cycles	275 ± 7.2	273 ± 10.1	07 ± 0.6

On the other hand, the Total Elongation (TE) dropped from about 21% in the natural ageing state to about 5% after the second cycle. Nevertheless, after four ARB cycles, a rise in the TE was attained to about 16% and then fell again in the fifth cycle. Herein, the tensile results for all the studied samples were concordant with the obtained microhardness ones as presented above.

In this context, this variation in mechanical properties can be attributed to two main factors: the applied heat treatments and plastic deformation. Indeed, the heat treatment carried out before rolling leads to the microstructure recrystallisation, dislocations mobility activation, and precipitates evolution. Moreover, the plastic deformation gives rise to the generation of dislocations, thus inducing the work hardening. Furthermore, with the increase of the ARB cycle, the grain refinement evolution is responsible for reducing the dislocations mean free path and its number of activity. There is a vital competition between several mechanisms: work hardening, grain refinement and dynamic recrystallisation which control the dislocations state (generation or annihilation) or grain size [31].

Consequently, as was reported, this competition affects the main strengthening precipitates when the dislocations are like the favourite nucleation sites for the major of these phases. Therefore, it alters the overall properties of the processed strips [45, 48].

Thus far, the grain refinement produced by SPD has been believed that it is the main reason for the strengthening of materials based on Hall–Petch relationship. Our results show that this understanding is not totally true. This conclusion was confirmed by Koizumi et al. [49] where they reported that softening of industrial pure aluminum processed by ECAP was observed at the ultralow strain rate of $\sim 10^{-7}$/s in uniaxial tensile tests despite the grain size refinement obtained. They conclude that the SPD processes decreases the athermal strength, and increases the viscosity of UFG materials.

In conclusion, the strength and ductility in the initial ARB stages are mainly influenced by establishing equilibrium between strain hardening, dislocations density and precipitates process. However, in the fourth cycle, which represents a transition state, the dynamic recrystallisation phenomenon was the dominant mechanism associated with grain refinement and precipitates state [31, 45].

The fracture mechanism. The SEM micrographs of the tensile fracture surfaces for the as-received and processed specimens are presented in Fig. 7. At low (L) magnification, the naturally aged sample (Fig. 7a-L) exhibits a slight necking when the micro-crack initiation and propagation were stared from the outer surface until attaining the global fracture towards the sample centre. At high (H) magnification, the fractography (Fig. 7a-H) exhibits a ductile fracture behaviour confirmed by a grey and fibrous appearance with the presence of deep dimpled structure developed from the nucleation, growth, and coalescence of microvoids following the classical void growth model [31, 46].

After the first ARB cycle, the tensile fractography (Fig. 7b-L) shows clearly the two individual layers with an apparent interface. From the second cycle, the last and the second last interfaces can be identified (Fig. 7c-L, 7d-L, 7e-L). In contrast, the interfacial bonding between the previous cycle interfaces has enhanced that conduct it to become indistinguishable with an appropriate metallurgical adhesion. This leads to assuming that the last and the second last bonding interfaces present the weakest zone in the processed strips, where the initiation and propagation of the micro-cracks will take place [31]. Also, a slight necking was observed in some individual layers, which means that the plastic deformation is not homogeneous across the samples thickness. Herein, it can be stated that the severely deformed strips and the narrowing are not similar in the whole cross-section of the processed specimens where each layer supports a distinct strain hardening, which leads to forming the basis of some types of micro-defects, such as void agglomerations and micro-cracks that lead to theirs
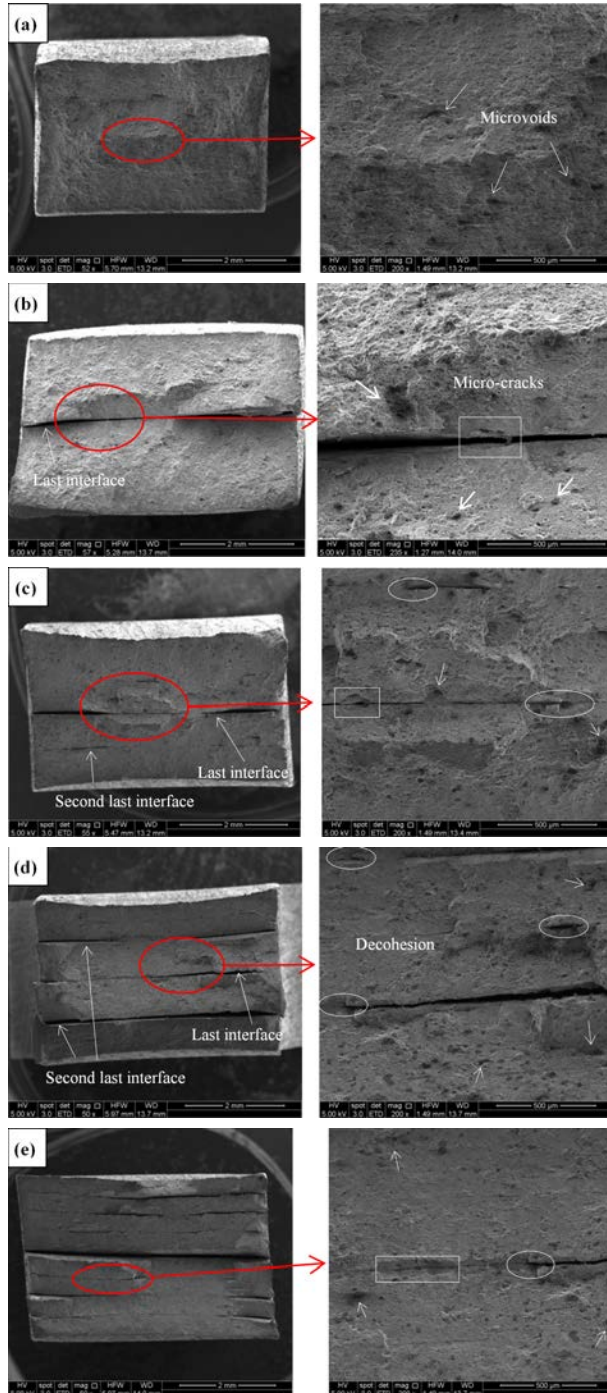
FIG. 7. SEM micrographs of tensile fractured surfaces of natural ageing and ARBed 2017A aluminium alloy at different number of cycles a) natural ageing, b) 1 cycle, c) 2 cycles, d) 4 cycles, and e) 5 cycles.

initiation and propagation from the outer surface, accordingly reduce the mechanical properties [46].

As a consequence, the processed strips behave like a laminate composite, in which the applied stress affects the individual layers rather than the entire sample. This can illustrate the stress distribution and its variation with necking or cracking in some layers. Consequently, the ductility and the strength were lower than those of the compact material.

Whereas, at high magnification (Fig. 7c-H, 7d-H, 7e-H), a variation in the dimples shape, size and orientation of the ARBed samples was perceived. Moreover, the micrographs exhibited that the average size and the number of dimples progressively decreased with increasing the number of ARB cycles when fine shear lips were detected due to the refining of grains, revealing that the failure type was a shear-ductile mixed mode [46, 47].

2.2.3. The compression test. The experimental compression true stress-strain curves for the studied specimens are shown in Fig. 8. The obtained compression curves can be divided into two stages: an initial linear elastic stage followed by a compacting stage that exhibited a considerable strain hardening phenomenon conducting to a linear rising in stress up to 50% of compressive strain. The average values of the Compressive Yield Stress (CYS) and Ultimate Compressive Strength (UCS) are given in Table 3.
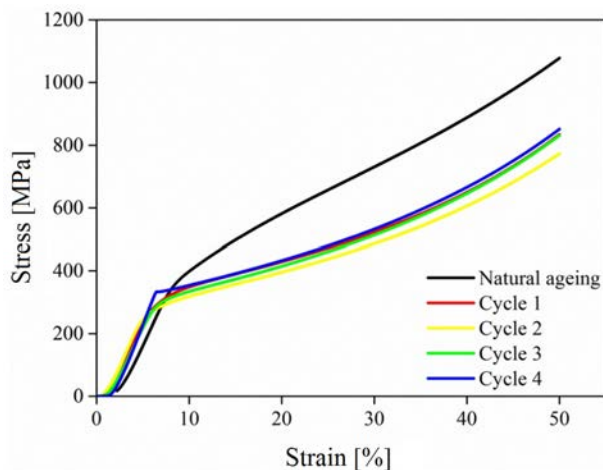

FIG. 8. Compression true stress-strain curves of natural ageing and ARB processed 2017A aluminium alloy under quasi-static loading.

According to these results, the natural ageing state has the maximum value of the UCS. In contrast, the ARBed samples showed stabilisation between 831 and 851 MPa for all cycles with a slight decrease to 773 MPa in the second cycle.

Table 3. Results of the compression test.

Specimen	UCS [MPa]	CYS [MPa]
Natural ageing	1078 $\pm$ 25	278 $\pm$ 2.1
1 cycle	834 $\pm$ 21	215 $\pm$ 2.1
2 cycles	773 $\pm$ 18	213 $\pm$ 2.0
3 cycles	831 $\pm$ 19	213 $\pm$ 2.0
4 cycles	851 $\pm$ 19	329 $\pm$ 2.5

Furthermore, for the three first cycles, the CYS value is constant and reaches an average of 214 MPa, but in the fourth cycle, an increase is observed up to 329 MPa which is the maximum value of CYS. However, the natural ageing state has a CYS value (278 MPa) lower than that of the fourth cycle and higher than the other cycles.

The quasi-static strength characteristics in the tensile and compression tests have a similar tendency. Both techniques confirmed the existence of a transient state in the fourth ARB cycle which exhibited the appropriate comprehensive mechanical properties resulting from the proper combination of the strain hardening, grain refinement, and high bonding quality. These mechanisms control the state of dislocations by controlling the number of barriers during the ARB process that influences the evolution of precipitates in the matrix and the refinement of grain size [48].

2.2.4. Mechanical behaviour under high strain rate. Figure 9 presents the true stress-strain curves for the studied specimens tested under dynamic impact loading. An elastic deformation was noticed at the beginning of the curves, followed
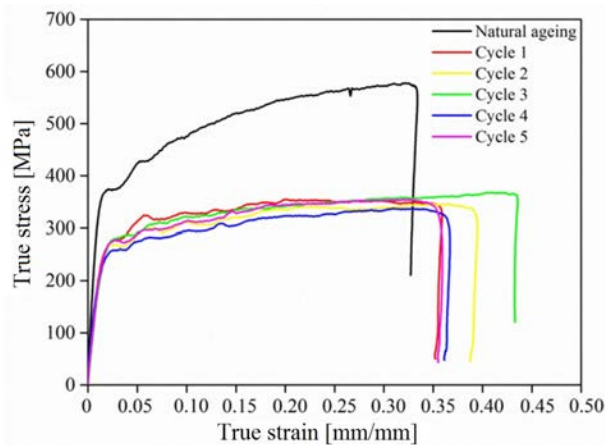

FIG. 9. SHPB true stress-strain curves of natural ageing and ARB processed 2017A aluminium alloy under dynamic loading.

by a transition zone after the true yield stress and, finally, a plastic deformation at the end of the curves, which corresponds to the samples strain hardening phenomena.

The SHPB curves show that, on the one hand, the as-received material exhibited the highest flow stress. On the other hand, stabilisation and decreased flow stress were observed for the ARBed samples at different cycles compared to the naturally aged sample.

The curves in Fig. 10 revealed a strain hardening rate drop, which indicates the domination effect of the thermal softening over the strain hardening. The
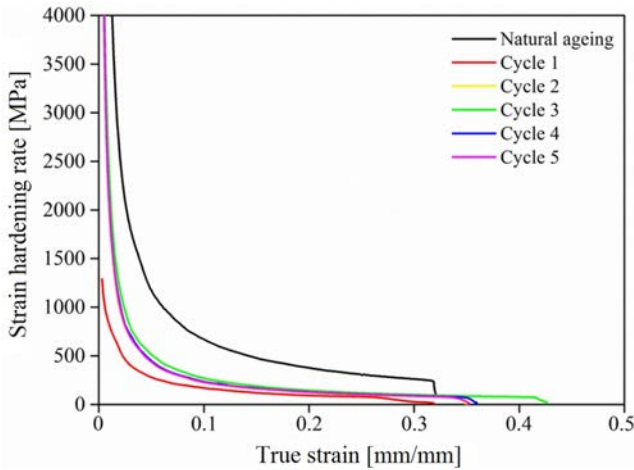

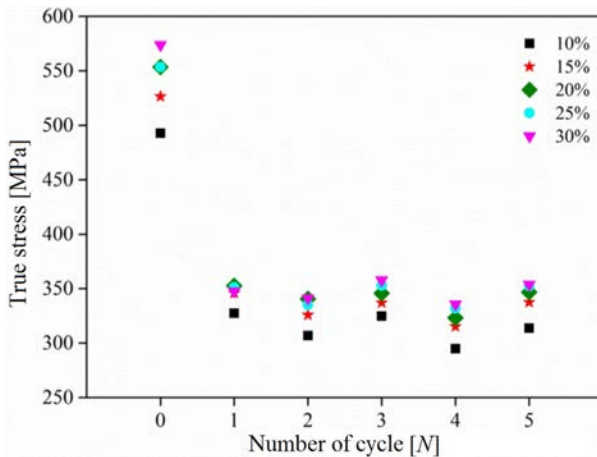FIG. 10. The strain hardening rate curves.

FIG. 11. True stress variation of natural ageing ($N = 0$) and ARBed 2017A aluminium alloy for different number of cycles at 10, 15, 20, 25 and 30% of true strain.
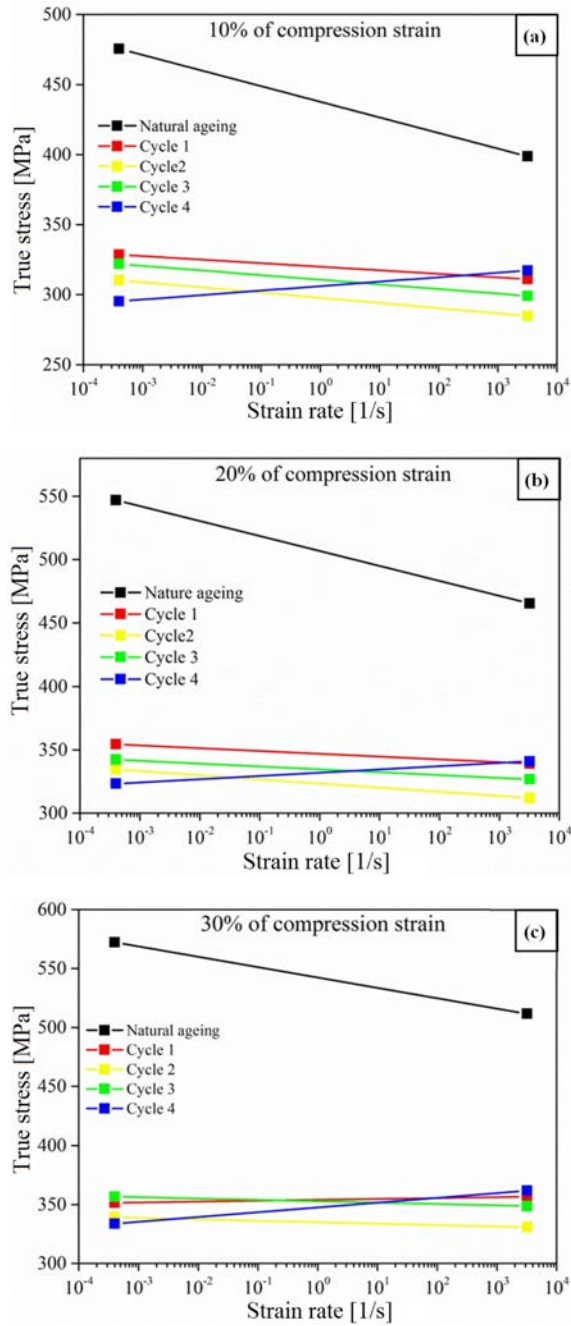
FIG. 12. True stress variation under quasi-static and dynamic loading for a) 10, b) 20 and c) 30% of true strain.

annihilation and rearrangement of dislocations can explain this drop due to the increase of temperature, resulting from the conversion from the plastic work into heat through the dynamic loading condition [48]. The thermal softening effect on the strain hardening behaviour under dynamic loading occurs in the true strain critical range between 0.01 and 0.05.

From Fig. 11, it can be stated that the naturally aged alloy presents the peak true stress value. Whereas, all curves have the same allure for the different ARBed specimens, presenting stability of the true stress between 300 and 350 MPa for the various true strain levels.

Figure 12 exhibits the variation of the true stress for the studied samples as a function of the strain rate ($4 \times 10^{-4}\,\text{s}^{-1}$ and $3200\,\text{s}^{-1}$) for 10, 20 and 30% from the true strain.

In the ARBed material, the strain rate does not have a noteworthy influence on the mechanical behaviour compared to the naturally aged material, where there was a considerable decrease in the stress under the dynamic conditions. That can be attributed to the thermal softening that overcomes the strain hardening in the as-received material with coarse grains; in addition to the thermal energy converted from the plastic work at the dynamic loading, the dislocations mobility increases and therefore the stress flow decreases [35, 40]. However, the equilibrium between thermal softening and strain hardening was established in the ARBed samples due to their microstructure evolution (grain refinement and precipitates state) which leads to conclude that the strain rate does not have a significant influence on the stress flow. Furthermore, a slight increase of the flow stress at the dynamic condition in the fourth cycle was observed, which confirmed the transition state reported above at this ARB cycle due to interfaces bonding enhancement and the dynamic recrystallisation mechanism.
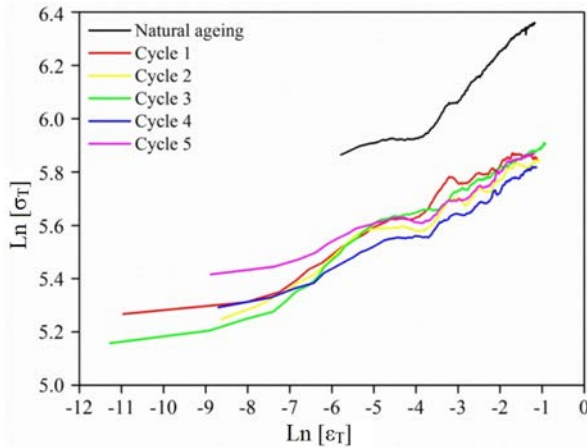

FIG. 13. The Ln-Ln plot of true stress-strain under dynamic loading of natural ageing and ARBed 2017A aluminium alloy.

Based on the development of the Hollomon law [13, 40], the strain hardening parameters for the studied strips showed in Table 4 are extracted from the linear fit line of the logarithm of the true stress versus the logarithm of the true strain curves (Fig. 13) under dynamic loading. These results demonstrate the stability of the hardening for the ARBed strips in different cycles which is around 0.073–0.08 and 363–399 for n (strain-hardening exponent) and K (strength coefficient), respectively. However, the as-received material exhibits the highest hardening values with a 0.136 strain-hardening exponent and 675 strength coefficient.

Table 4. **Strain hardening parameters of studied samples.**

Specimen	n	K
Natural ageing	0.136	675
1 cycle	0.080	399
2 cycles	0.079	377
3 cycles	0.083	394
4 cycles	0.079	363
5 cycles	0.073	381

3. Experimental methods

The chemical composition of the as-received sheets of 2017A-T4 aluminium alloy (solution heat-treated and naturally aged) is listed in Table 5.

Table 5. **Chemical composition of 2017A aluminium alloy [wt. %].**

Elements	Mg	Cu	Mn	Fe	Si	Al
Wt. %	1.05	4.05	0.49	0.27	0.45	93.70

In order to improve the interface bonding, the as-received strips for the ARB process with the dimensions of $300\,\text{mm} \times 150\,\text{mm} \times 4\,\text{mm}$ were degreased in acetone and wire brushing before stacking; then, they were strongly fixed using steel wires. Subsequently, the sheets were heated at 300°C for 15 min to improve the workability, favourite high bonding quality and reduce the accumulative strain. Afterwards, the sheets were subjected to 50% reduction per cycle to a final thickness of 4 mm. The bonded strips were cut into two similar pieces; then, this procedure was repeated up to five cycles. The schematic illustration of the ARB process to produce strips up to 32 layers is shown in Fig. 14. The ARB process was performed without lubricant on a laboratory rolling mill with a diameter of 500 mm at a roller speed of 600 rpm. The ARB process parameters are summarised in Table 6.
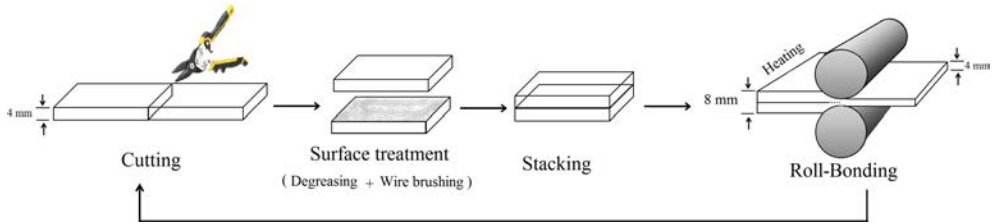
FIG. 14. Principle of the Accumulative Roll Bonding (ARB) process.

Table 6. Roll-bonding parameters.

Heating	Roll diameter	Roll speed	Initial thickness (t_0)	Reduction in each cycle	Number of cycles
300°C/15 min	500 mm	600 rpm	4 mm	50%	1 to 5

The metallographic observation samples were prepared through conventional mechanical with Silicon Carbide Grinding papers and then electrolytic polishing using the A2 Struers electrolyte at 39 V for 20 s. The Olympus GX53 inverted optical microscope was employed to analyse the bonding quality between several prepared sample layers. To examine the evolution of the grain specifications at the different number of cycles, Electron Back Scattering Diffraction (EBSD) measurements were carried out using the TSL OIM software in FEG-SEM SUPRA 55 VP Scanning Electron Microscope (SEM) operating at 20 KV. An average of 5 Vickers micro-hardness measurements at different points were obtained by the HWDM-1 micro-hardness tester under the load of 300 g for 15 s. Tensile test specimens were cut along the rolling direction (RD) by wire electro-erosion technique according to ASTM Standard B 557M. All the tensile values were obtained from the average of three tests. The tensile test was performed at ambient temperature on an EZ20 testing machine at a crosshead speed of 0.1 mm/min. The dimensions of the tensile specimen are shown in Fig. 15.
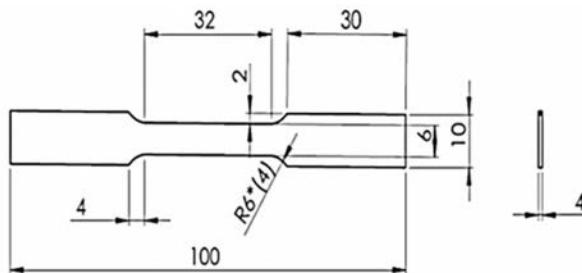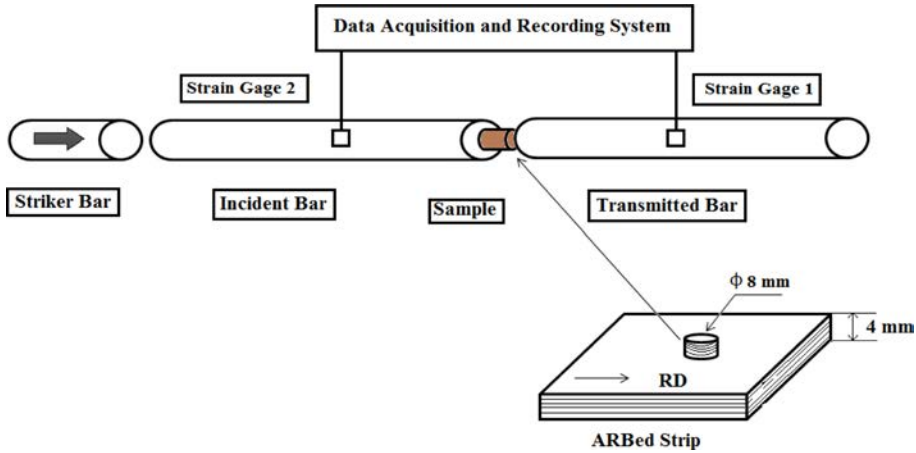

FIG. 15. Tensile test specimen.

Fig. 16. Schematic of Split–Hopkinson Pressure Bar (SHPB) equipment.

Cylindrical samples with 8 mm in diameter and 4 mm in length were prepared for the compression test at room temperature under quasi-static (strain rate of 4×10^{-4}) and dynamic (strain rate of $3200\,\mathrm{s}^{-1}$) loading conditions by using the universal testing machine and the Split–Hopkinson Pressure Bar system (SHPB) shown in Fig. 16, respectively.

4. Conclusions

In the present study, the UFGs 2017A aluminium alloy (Al-Cu-Mg) was successfully produced from the T4 temper condition (natural ageing) using the ARB process for up to five cycles. The deformation behaviour under both the quasi-static and dynamic loadings was studied. Based on the above investigations, the following conclusions can be drawn:

1. The optical micrographs show an excellent bonding between the individual layers for all the ARBed strips. The different layers were characterised as homogeneous, parallel and having identical thickness along with the interface with no delamination or cracks except in the last interface of the fifth cycle, where a slight loss of cohesion was observed.

2. The SEM micrographs revealed the presence of precipitates (Al_2Cu, Al_2CuMg) with differences in shape and sizes. The configuration of these precipitates changed during the ARB process, which becomes finer and distant as a function of the number of cycles.

3. In the EBSD results a lamellar structure was observed in the three first ARB cycles due to severe plastic deformation. The spacing of lamellar boundaries decreased with increasing the number of ARB cycles. Beyond that, the lamellar

structure changed to an ultrafine grain structure with an average grain size up to $1.7\,\mu\mathrm{m}$ at the fifth cycle.

4. The microhardness and strength (yield and ultimate tensile) measurements of all specimens exhibit that the natural ageing alloy had the highest values and a significant reduction in the ARB processed alloy. Saturation in microhardness was remarked in the three first ARB cycles, followed by a slight decrease thereafter. Moreover, the tensile test results revealed a decrease of strengthening until the fourth cycle and then it increased towards the same level at the first cycles.

5. The fracture surface analyses of ARB processed material reveal that the failure mode was a shear ductile fracture. Moreover, it behaves like a laminate in which tensile stress acts on the individual layers rather than the compact material.

6. The mechanical characterisation by a compression test was done at two strain rates: $3200\,\mathrm{s}^{-1}$ (dynamic) and $4\times10^{-4}\,\mathrm{s}^{-1}$ (quasi-static). The strain hardening behaviour of ARBed samples showed a lower strain hardening exponent and strain hardening rate compared to the natural ageing sample. The domination of thermal softening overstrain hardening was clearly observed at a high strain rate due to the conversion of kinetic energy to thermal energy. Besides, the influence of the strain rate on work hardening as a function of the number of ARB cycles was not important.

7. In addition to plastic deformation, thermal energy and dynamic recrystallisation phenomena, the evolution of precipitates during the ARB process into the 2017A-T4 aluminium alloy played an important role in the dislocations progression and thus on the decrease in the mechanical properties of the processed alloy, owing to the fact that the dislocations are like the favourite nucleation sites for the most of precipitates.

Thus, there are other parameters besides a grain size that influence the hardening of SPDed materials. The present work shows that the conditions of the SPD process (heating conditions before roll bonding: $T = 350°\mathrm{C}$, $t = 15\,\mathrm{min}$), composition and microstructure of a started material (natural ageing state of 2017A aluminium alloy) play an important role on the mechanical behaviour of the materials grain refined.

References

1. S. Lee, P.B. Berbon, M. Furukawa, Z. Horita, M. Nemoto, N.K. Tsenev, R.Z. Valiev, T.G. Langdon, *Developing superplastic properties in an aluminium alloy through severe plastic deformation*, Materials Science and Engineering A, **272**, 63–72, 1999, https://doi.org/10.1016/S0921-5093(99)00470-0.

2. R.Z. Valiev, A.V. Korznikov, R.R. Mulyukov, *Structure and properties of ultrafine-grained materials produced by severe plastic deformation*, Materials Science and Engineering A, **168**, 141–148, 1993, https://doi.org/10.1016/0921-5093(93)90717-S.

3. A. Azushima, R. Kopp, A. Korhonen, D.Y. Yang, F. Micari, G.D. Lahoti, P. Groche, J. Yanagimoto, N. Tsuji, A. Rosochowski, A. Yanagida, *Severe plastic deformation (SPD) processes for metals*, CIRP Annals – Manufacturing Technology, **57**, 716–735, 2008, http://dx.doi.org/10.1016/j.cirp.2008.09.005.

4. N. Hansen, *Hall–Petch relation and boundary strengthening*, Scripta Materialia, **51**, 801–806, 2004, https://doi.org/10.1016/j.scriptamat.2004.06.002.

5. D. J. Abson, J.J. Jonas, *The Hall-Petch relation and high-temperature subgrains*, Metal Science Journal, **4**, 1970, https://doi.org/10.1179/msc.1970.4.1.24.

6. M. Furukawa, Z. Horita, M. Nemoto, R.Z. Valiev, T.G. Langdon, *Microhardness measurements and the Hall-Petch relationship in an Al-Mg alloy with submicrometer grain size*, Acta Materialia, **44**, 11, 4619–4629, 1996, https://doi.org/10.1016/1359-6454(96)00105-X.

7. T. Koizumi, M. Kuroda, *Grain size effects in aluminium processed by severe plastic deformation*, Materials Science and Engineering A, **710**, 300–308, 2018, https://doi.org/10.1016/j.msea.2017.10.077.

8. R.G. Guan, D. Tie, *A review on grain refinement of aluminum alloys: progresses, challenges and prospects*, Acta Metallurgica. Sinica, **30**, 409–432, 2017, http://doi.org/10.1007/s40195-017-0565-8.

9. R.Z. Valiev, R.K. Islamgaliev, I.V. Alexandrov, *Compact nanostructured materials from severe plastic deformation*, Progress in Materials Science, **45**, 103–189, 2000, http://doi.org/10.1016/S0079-6425(99)00007-9.

10. R.Z. Valiev, Y. Estrin, Z. Horita, T.G. Langdon, M.J. Zehetbauer, Y.T. Zhu, *Producing compact ultrafine-grained materials by severe plastic deformation*, JOM: Journal of the Minerals, Metals & Materials Society (TMS), **58**, 33–39, 2006, http://dx.doi.org/10.1007/s40195-017-0565-8.

11. E. Darmiani, I. Danaee, M.A. Golozar, M.R. Toroghinejad, *Corrosion investigation of Al–SiC nano-composite fabricated by accumulative roll bonding (ARB) process*, Journal of Alloys and Compounds, **552**, 31–39, 2013, http://dx.doi.org/10.1016/j.jallcom.2012.10.069.

12. Y.F. Sun, N. Tsuji, H. Fujii, F.S. Li, *Cu/Zr nanoscaled multi-stacks fabricated by accumulative roll bonding*, Journal of Alloys and Compounds, **504**, 443–447, 2010, http://dx.doi.org/10.1016/j.jallcom.2010.02.201.

13. G.G. Maier, E.G. Astafurova, H.J. Maier, E.V. Naydenkin, G.I. Raab, P.D. Odessky, S.V. Dobatkin, *Annealing behaviour of ultrafine grained structure in low-carbon steel produced by equal channel angular pressing*, Materials Science and Engineering A, **581**, 104–107, 2013, http://dx.doi.org/10.1016/j.msea.2013.05.075.

14. E. Mostaed, A. Fabrizi, D. Dellasega, F. Bonollo, M. Vedani, *Microstructure, mechanical behaviour and low temperature superplasticity of ECAP processed ZM21 Mg alloy*, Journal of Alloys and Compounds, **638**, 267–276, 2015, http://dx.doi.org/10.1016/j.jallcom.2015.03.029.

15. M. Besterci, T. Kvačkaj, R. Kočiško, J. Bacsó, K. Sulleiová, *Formation of ultrafine-grained (UFG) structure and mechanical properties by severe plastic deformation (SPD)*, Metalurgija, **47**, 4, 295–299, 2008.

16. F. Khodabakhshi, M. Haghshenas, H. Eskandari, B. Koohbor, *Hardness-strength relationships in fine and ultra-fine grained metals processed through constrained groove pressing*, Materials Science and Engineering A, **636**, 331–339, 2015, http://dx.doi.org/10.1016/j.msea.2015.03.122.

17. J. Zrnik, T. Kovarik, Z. Novy, M. Cieslar, *Ultrafine-grained structure development and deformation behaviour of aluminium processed by constrained groove pressing*, Materials Science and Engineering A, **503**, 126–129, 2009, https://doi.org/10.1016/j.msea.2008.03.050.

18. E. Hosseini, M. Kazeminezhad, *Nanostructure and mechanical properties of 0–7 strained aluminium by CGP: XRD, TEM and tensile test*, Materials Science and Engineering A, 526, 219–224, 2009, https://doi.org/10.1016/j.msea.2009.07.028.

19. N. Kamikawa, N. Tsuji, *Microstructure and mechanical properties of ARB processed aluminium with different purities*, Materials Transactions, **57**, 10, 1720–1728, 2016, https://doi.org/10.2320/matertrans.MH201519.

20. Y. Saito, H. Utsunomiya, N. Tsuji, T. Sakai, *Novel ultra-high straining process for compact materials-development of the accumulative Roll-Bonding (ARB) process*, Acta Materialia, **47**, 2, 579–583, 1999, https://doi.org/10.1016/S1359-6454(98)00365-6.

21. A.M. Faradonbeh, M. Shamanian, H. Edris, M. Paidar, Y. Bozkurt, *Friction stir welding of Al-B$_4$C composite fabricated by accumulative roll bonding: evaluation of microstructure and mechanical behaviour*, Journal of Materials Engineering and Performance, **27**, 835–846, 2018, https://doi.org/10.1007/s11665-018-3131-2.

22. M. Yousefieh, M. Tamizifar, S.M.A. Boutorabi, E. Borhani, *An investigation on the microstructure, texture and mechanical properties of an optimized friction stir welded ultrafine-grained Al–0.2 wt% Sc alloy deformed by accumulative roll bonding*, Journal of Materials Science, **53**, 4623–4634, 2018, https://doi.org/10.1007/s10853-017-1897-5.

23. A. Salimi, E. Borhani, E. Emadoddin, *Evaluation of mechanical properties and structure of 1100-al reinforced with zro$_2$ nano-particles via accumulatively roll-bonded*, Procedia Materials Science, **11**, 67–73, 2015, https://doi.org/10.1016/j.mspro.2015.11.094.

24. Y. Saito, N. Tsuji, H. Utsunomiya, T. Sakai, R.G. Hong, *Ultra-fine grained compact aluminum produced by Accumulative Roll-Bonding (ARB) process*, Scripta Materialia, **39**, 9, 1221–1227, 1998, https://doi.org/10.1016/S1359-6462(98)00302-9.

25. K.T. Ramesh, *Nanomaterials Mechanics and Mechanisms*, Springer, 2009, https://doi.org/10.1007/978-0-387-09783-1.

26. C.W. Schmidt, P. Knödler, H.W. Höppel, M. Göken, *Particle based alloying by accumulative roll bonding in the system Al-Cu*, Metals, **1**, 65–78, 2011, https://doi.org/10.3390/met1010065.

27. S.H. Lee, Y. Saito, N. Tsuji, H. Utsunomiya, T. Sakai, *Role of shear strain in ultragrain refinement by accumulative roll-bonding (ARB) process*, Scripta Materialia, **46**, 281–285, 2002, https://doi.org/10.1016/S1359-6462(01)01239-8.

28. N. Tsuji, Y. Saito, S.H. Lee, Y. Minamino, *ARB (ACCUMULATIVE Roll-Bonding) and other new techniques to produce compact ultrafine grained materials*, Advanced Engineering Materials, **5**, 5, 2003, https://doi.org/10.1002/adem.200310077.

29. X. Huang, N. Tsuji, N. Hansen, Y. Minamino, *Microstructural evolution during accumulative roll-bonding of commercial purity aluminium*, Materials Science and Engineering A, 340, 265–271, 2003, https://doi.org/10.1016/S0921-5093(02)00182-X.

30. W. Skrotzki, J. Scharnweber, C.G. Oertel, H.W. Höppel, I. Topic, H.G. Brokmeier, J. Jaschinski, *Plastic anisotropy of ultrafine grained Al alloy AA6016 produced by accumulative roll bonding*, Solid State Phenomena, **160**, 171–176, 2010, https://doi.org/10.4028/www.scientific.net/SSP.160.171.

31. M. Alvand, M. Naseri, E. Borhani, H. Abdollah-Pour, *Nano/ultrafine grained AA2024 alloy processed by accumulative roll bonding: a study of microstructure, deformation texture and mechanical properties*, Journal of Alloys and Compounds, **712**, 517–525, 2017, http://dx.doi.org/10.1016/j.jallcom.2017.04.117.

32. R. Z. Valiev, Y. Estrin, Z. Horita, T.G. Langdon, M.J. Zehetbauer, Y.T. Zhu, *Fundamentals of superior properties in compact NanoSPD materials*, Materials Research Letters, **4**, 1–21, 2016, http://dx.doi.org/10.1080/21663831.2015.1060543.

33. S.H. Lee, Y. Saito, T. Sakai, H. Utsunomiya, *Microstructures and mechanical properties of 6061 aluminium alloy processed by accumulative roll-bonding*, Materials Science and Engineering A, **325**, 228–235, 2002, https://doi.org/10.1016/S0921-5093(01)01416-2.

34. S. O. Gashti, A. Fattah-alhosseini, Y. Mazaheri, M. K. Keshavarz, *Effects of grain size and dislocation density on strain hardening behaviour of ultrafine grained AA1050 processed by accumulative roll bonding*, Journal of Alloys and Compounds, **658**, 854-861, 2016, https://doi.org/10.1016/j.jallcom.2015.11.032.

35. J. Shahbazi Karami, S. Sepahi-Boroujeni, M. Khodsetan, *Investigating the effects of Expansion Equal Channel Angular Extrusion (Exp-ECAE) on dynamic behavior of AA7075 aluminum alloy,* International Journal of Advanced Design and Manufacturing Technology, **9**, 3, 11–18, 2016.

36. J. Jiang, J. Shi, Y. Yao, A. Ma, D. Song, D. Yang, J. Chen, F. Lu, *Dynamic compression properties of an ultrafine-grained Al-26 wt.% Si alloy fabricated by equal-channel angular pressing*, Journal of Materials Engineering and Performance, **24**, 2016–2024, 2015, https://doi.org/10.1007/s11665-015-1455-8.

37. P. Henrique, R. Pereira, Y.C. Wang, Y. Huang, T.G. Langdon, *Influence of grain size on the flow properties of an Al-Mg-Sc alloy over seven orders of magnitude of strain rate*, Materials Science and Engineering A, **685**, 367–376, 2017, http://dx.doi.org/10.1016/j.msea.2017.01.020.

38. M. A. Afifi, P. Henrique, R. Pereira, Y.C. Wang, Y. Wang, S. Li, T.G. Langdon, *Effect of ECAP processing on microstructure evolution and dynamic compressive behaviour at different temperatures in an Al-Zn-Mg alloy*, Materials Science and Engineering A, **684**, 617–625, 2017, http://dx.doi.org/10.1016/j.msea.2016.12.099.

39. A.N. Petrova, I.G. Brodova, S.V. Razorenov, E. V. Bobruk, *Grain size effects on quasi-static and dynamic strength of ultrafine-grained Al-Mg-Mn Alloy produced by high-pressure torsion*, Journal of Materials Engineering and Performance, **29**, 464–469, 2020, https://doi.org/10.1007/s11665-019-04511-3.

40. A. Azimi1, G.M. Owolabi, H. Fallahdoost, N. Kumar, G. Warner, *Dynamic failure investigation in ultrafine grained AA2219: mechanical and microstructural analysis*, Metals and Materials International, **25**, 900–911, 2019, https://doi.org/10.1007/s12540-019-00254-x.

41. K.V. IVANOV, S.V. RAZORENOV, G.V. GARKUSHIN, *Quasi-quasi-static and shock-wave loading of ultrafine-grained aluminium: effect of microstructural characteristics*, Journal of Materials Science, **53**, 14681–14693, 2018, https://doi.org/10.1007/s10853-018-2619-3.

42. C. SIGLI, F. DEGEUSER, A. DESCHAMPS, J. LÉPINOUX, M. PEREZ, *Recent advances in the metallurgy of aluminum alloys. Part II: Age hardening Développements récents en métallurgie des alliages d'aluminium. Deuxième partie: durcissement par revenu*, Comptes Rendus Physique, **19**, 8, 688–709, 2018, https://doi.org/10.1016/j.crhy.2018.10.012.

43. L. HEMMOUCHE, C. FARES, M.A. BELOUCHRANI, *Influence of heat treatments and anodization on fatigue life of 2017A alloy*, Engineering Failure Analysis, **35**, 554–561, 2013, https://doi.org/10.1016/j.engfailanal.2013.05.003.

44. C. FARES, L. HEMMOUCHE, M.A. BELOUCHRANI, D. CHICOT, E.S, PUCHI-CABRERA, *Coupled effects of substrate microstructure and sulphuric acid anodizing on fatigue life of a 2017A aluminum alloy*, Materials and Design, **86**, 723–734, 2015, https://doi.org/10.1016/j.matdes.2015.07.120.

45. A. DESCHAMPS, F. DE GEUSER, Z. HORITA, S. LEE, G. RENOU, *Precipitation kinetics in a severely plastically deformed 7075 aluminium alloy*, Acta Materialia, **66**, 105–117, 2014, http://dx.doi.org/10.1016/j.actamat.2013.11.071.

46. S. PASEBANI, M.R. TOROGHINEJAD, *Nano-grained 70/30 brass strip produced by accumulative roll-bonding (ARB) process*, Materials Science and Engineering A, **527**, 491–497, 2010. http://dx.doi.org/10.1016/j.msea.2009.09.029.

47. A. MEDJAHED, B. LI, L. HOU, R. WU, A. ZEGAOUI, M. DERRADJI, H. BENYAMINA, *Evolution of microstructure, mechanical properties, and thermal conductivity of an Al-Li-Cu-Mg-Zr alloy processed by Accumulative Roll Bonding (ARB)*, JOM: the Journal of the Minerals, Metals & Materials Society (TMS), **71**, 4096–4104, 2019, https://doi.org/10.1007/s11837-019-03646-x.

48. A.A. TIAMIYU, A.Y. BADMOS, A.G. ODESHI, *Effects of temper condition on high strain-rate deformation of AA 2017 aluminum alloy in compression*, Materials and Design, **89**, 872–883, 2016, https://doi.org/10.1016/j.matdes.2015.10.047.

49. T. KOIZUMI, A. KURUMATANI, M. KURODA, *Athermal strength of pure aluminum is significantly decreased by severe plastic deformation and it is markedly augmented by subsequent annealing*, Scientific Reports, **10**, 14090, 2020, https://doi.org/10.1038/s41598-020-70160-5.